Department of Companion Animals and Horses

University of Veterinary Medicine Vienna

Clinic of Small Animal Surgery

(Head: Univ. Prof. Dr. med. vet. Eva Schnabl-Feichter, Dipl. ECVS)

Virtual suboccipital craniotomy approach in cats

Diploma thesis submitted for the fulfillment of the requirements for the degree of

MAGISTRA MEDICINAE VETERINARIAE (Mag. med. vet.)

University of Veterinary Medicine Vienna

submitted by

Susanna Szelestey

Vienna, February 2023

Supervisor: Dr.med.vet. Gabriele Gradner, Dipl. ECVS
Clinic of Small Animal Surgery
University Clinic for Small Animals
University of Veterinary Medicine Vienna

Appraiser: Priv.-Doz. Dr.med.vet. Akos Pakozdy, Dipl. ECVN
Clinical Unit of Internal Medicine Small Animals
University Clinic for Small Animals
University of Veterinary Medicine Vienna

Contents

1 Abbreviations

App 1 ..... standard approach for suboccipital craniotomy
App 2 left ..... extended approach to the left for suboccipital craniotomy
App 2 right ..... extended approach the the right for suboccipital craniotomy
CT ..... computed tomography
Fig. ..... figure
For. ..... Foramen
HemL ..... left hemisphere of the cerebellum
HemR ..... right hemisphere of the cerebellum
ICP ..... intercranial pressure
M. ..... Musculus
MR ..... magnetic resonance
MRI ..... magnetic resonance imaging
MV ..... main value, average
PMMA ..... polymethylmethacrylate
Proc. ..... Processus
SD ..... standard deviation
Tab. ..... table

2 Introduction

Craniotomy is a surgical procedure creating a defect in the calvarium in order to access the brain. There are different kinds of surgical approaches used in veterinary medicine. Lateral also known as rostrotentorial, transfrontal and suboccipital craniotomy being the most commonly used ones. To provide increased exposure to the brain, the procedures can also be combined. (Fossum 2019)

Depending on the location and size of the approach, the bone flap that is created during craniotomy can either be repositioned (craniotomy) or not replaced (craniectomy). For limited approaches with a small bony defect, the bone flap is not usually replaced in cats. In extensive craniotomy, such as transfrontal craniotomy or combined approaches, a bony reconstruction is likely necessary. Moreover other methods such as calvarial allografts, titanium mesh or the use of polymethylmethacrylate (PMMA) are described to close the bony defect. (Langley-Hobbs et al. 2014,Shores and Brisson 2017)

One of the most common indication for intracranial surgery is brain tumor excision. Due to the increasing availability of advanced diagnostic imaging such as computed tomography (CT) and magnetic resonance imaging (MRI), a rising number of intracranial neoplasia can be appropriately diagnosed and specifically treated. According to literature the incidence of intracranial tumors in cats is approximately 3.5 per 100.000 cats. Meningioma is reported to be the most commonly found primary neoplasia, with a frequency of 58%. (Troxel et al 2003) Other reasons for craniotomy include decompression to control the intracranial pressure, removal of injured brain tissue and bone fragments that occur after traumatic injuries, drainage of abscesses and treatment of congenital anomalies. (Langley-Hobbs et al. 2014)

Most reports and books focus on craniotomy approaches in dogs and only few describe the special features of the feline calvarium. Particularly suboccipital craniotomy is often used to establish foramen magnum decompression in dogs with Chiari-like malformation. (Shores and Brisson 2017) There is only little information available on which craniotomy approaches are practicable in cat.

This diploma thesis will focus on the suboccipital craniotomy approach in cats. The aim is to describe bony landmarks to standardize the maximum expansion of the approach so that as much of the structures of the cerebellum as possible can be made visible without insulting vital structures. The difference in accessibility to the cerebellum between a standard suboccipital approach and a rostrolaterally extended approach on the left and on the right side, respectively, was captured. I hypothesize that only a small part of the cerebellum is

accessible through a standard suboccipital approach and that the accessibility is significantly increased, when the craniotomy approach is rostrolaterally extended. However, it must be evaluated how much increase in visibility of the cerebellum can be achieved on either side without substantially insulting vital structures. In literature the rostrolaterally extended approach is usually referred to as a combined rostrotentorial and suboccipital approach. (Bagley et al. 1997) In order to do so, a virtual craniotomy using the Amira® software will be executed.

2.1 Anatomy of the feline skull

In order to carry out a craniotomy successfully, precise knowledge of anatomical structures is needed. Due to less overlaying muscles and a thinner calvarium, the feline skull is mildly more accessible than the canine skull. (Langley-Hobbs et al. 2014) Since this thesis only covers the suboccipital approach, the following descriptions will focus on the caudal aspect of the feline skull.

2.1.1 Skeleton of the head

The skull can be divided into two segments. The *Cranium* encloses the brain with its membranes and vessels and was formerly called *Neurocranium.* The second part is called *Facies* and surrounds parts of the digestive and respiratory system. Both parts are composed of a number of small bones, which are connected through sutures. Together those bones form the cranial cavity, the *Cavum cranii*. The dorsal aspect of the skull is called *Calvarium* and consists of the paired *Os frontale* and *Os parietale,* the unpaired interparietal bone and a part of the occipital bone. Laterally to those the *Os temporale* continues. The basis of the *Cranium* is constructed out of *Os basispenoidale*, *Os presphenoidale* and *Pars basilaris* of the occipital bone. The internal surface of the *Basis cranii* carries three pits, *Fossa cranii rostralis, media and caudalis*. Towards the neck the brain is protected by the occipital bone. The *Os ethmoidale* borders the *Cavum cranii* towards the nasal cavity. (Salomon 2015, Consantinescu 2018, König und Liebich 2005)

The parietal and frontal bones are joined by sutures. The point where the transverse and sagittal suture meet, is called *Bregma*. Caudally, the parietal and occipital bones are connected through the sagittal and lambdoid sutures. The meeting of those two sutures is called *Lambda*. *Bregma* and *Lambda* serve as two important surgical landmarks in intracranial surgery in dogs. *Bregma* can be difficult to identify on the feline skull. Other easily detectable anatomical landmarks on the feline skull include the frontal process of the zygomatic bone, the external occipital protuberance, the nuchal crest and many more.(Filgueiras 2016, Zilli et al. 2021, Kent et al. 2020)

The occipital bone can be divided into three sections. *Pars basilaris* and *Pars lateralis* surround the *Foramen (For.) magnum*, which connects the cranial cavity with the vertebral canal and contains the *Medulla oblongata*. *Pars basilaris* reaches from the *For. magnum* to the basisphenoid bone and forms the caudal aspect of the *Basis cranii*. The flexor muscles of the head insert at the *Tuberculum musculare*, which is located ventrally on the outer surface of *Pars basilaris*. The *Pars lateralis* forms two *Condyli occipitales* for the articulation with the atlas. The *Fossa condylaris dorsalis* is a depression dorsal to the occipital condyle. Laterally to the *Condylus occipitalis* the *Processus (Proc.) jugularis* is located. From this process the *Processus paracondylaris* protrudes ventrally and serve as an apophysis for muscular attachment. The *Fossa condylaris ventralis*, which is where the *Canalis nervi hypoglossi* ends, is located between *Condylus occipitalis* and *Proc. paracondylaris*. *Pars basilaris* also forms an *Incisura jugularis*, which borders the *For. jugulare* together with the *Pars petrosa* of the temporal bone. The third and dorsal part of the occipital bone is called *Squama occipitalis*. The *Protuberatia occipitalis externa* protrudes median on the external surface of the squama. The crest that reaches from *Protuberatia occipitalis externa* to *For. magnum* is called *Crista occipitalis externa*, which serves as a muscular attachment point for the extensor muscles. On both sides is a sharp transverse crest, called *Crista nuchae*. The *Crista nuchae* continues ventrally as the *Crista supramastoidea*, which is a part of the temporal bone. The *Crista saggitalis externa* is a sagittal crest that protrudes from the dorsal surface of the Squama and continues rostrally on the frontal bone. (Salomon 2015, Constantinescu 2018)

The interparietal bone is an unpaired bone that lies rostral to the occipital bone between the two parietal bones. It fuses with the occipital bone and forms the *Proc. interparietalis*. On the internal surface, a *Proc. tentoricus* is located. Together with the process of the same name formed by the occipital and the parietal bones, it forms the *Tentorium cerebelli osseum*. (Salomon 2015)

The *Os temporale* consists of three parts. *Pars petrosa*, or petrosal bone, encloses the inner ear and vestibular system. Caudal to the external auditory meatus, it forms the *Proc. mastoideus*, which is where the hyoid bone attaches. Dorsally to the process the *For. mastoideum* is located. Pars tympanica, which is located ventrally, and Pars squamosa, which creates the basal lateral wall of the *Cranium*, are the other two parts of the temporal bone. (Salomon 2015, Constantinescu 2018, Nickel 2005)

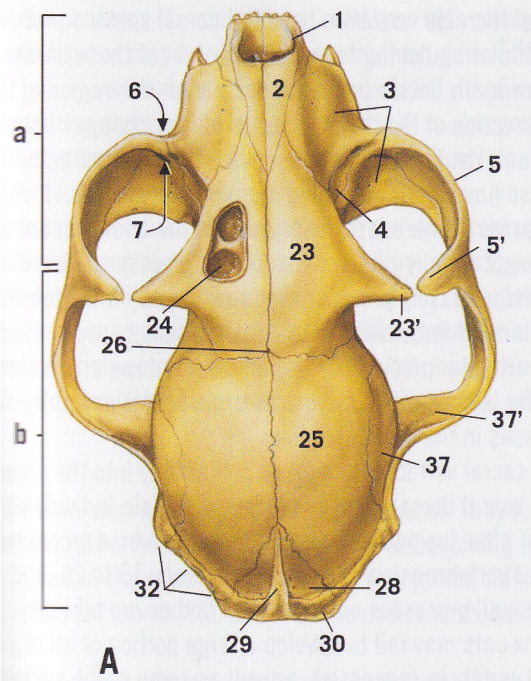

Fig. 1: Skull, dorsal view; a) bones of the face b) bones of the cranium 1 Incisive bone 2 Nasal bone 3 Maxilla 4 Lacrimal bone 5 Zygomatic bone 5′ Its frontal process 6 Infraorbital foramen 7 Maxillary foramen 23 Frontal bone 23′ Its zygomatic process 24 Frontal sinus 25 Parietal bone 26 Bregma 28 Interparietal bone 29 Sagittal crest 30 Occipital bone 32 Nuchal crest 37 Temporal bone 37′ Its zygomatic process (Hudson and Hamilton 2010)

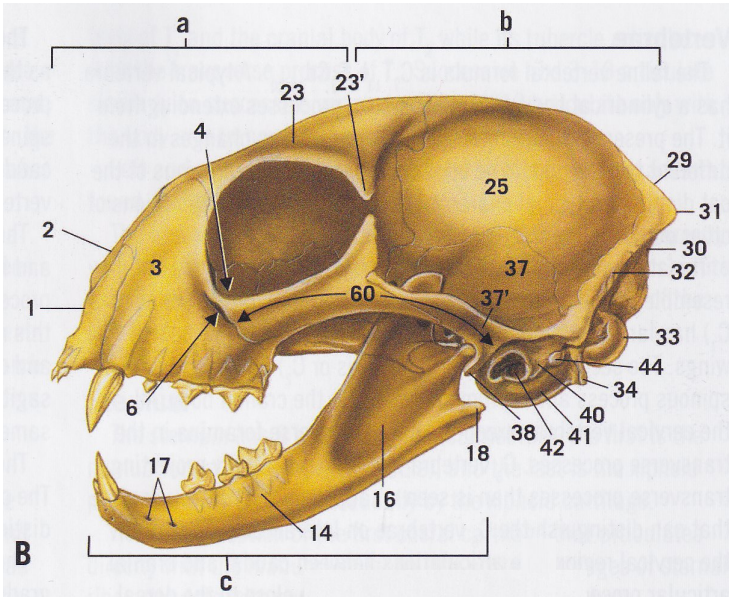

Fig. 2: Skull with mandible, left lateral view; a) Bones of the face b) bones of the cranium c) Mandible 1 Incisive bone 2 Nasal Bone 3 Maxilla 4 Lacrimal bone 6 Infraorbital foramen 14 Body of the mandible 16 Masseteric fossa 17 Mental foramina 18 Angular process 23 Frontal bone 23′ Its zygomatic process 25 Parietal bone 29 Sagittal crest 30 Occipital bone 31 External occipital protuberance 32 Nuchal crest 33 Occipital condyle 34 Paracondylar process 37 Temporal bone, squamous part 37′ Its zygomatic process 38 Retroarticular process 40 Temporal bone, tympanic part 41 Tympanic bulla 42 External acoustic meatus 44 Mastoid process (Hudson and Hamilton 2010)

2.1.2 Muscles of the head

Directly beneath the skin in the neck region lies the *Platysma*, which is a muscle plate that radiates into the facial muscles. Several head muscles insert into parts of the occipital bone. *Musculus (M:) rectus capitis dorsalis major* lies dorsally and reaches from *Proc. spinosus axis* to *Squama occipitalis*. *M. rectus capitis dorsalis minor* lies ventrally to the preceding muscle and reaches from *Tuberculum dorsale atlantis* to *Squama occipitalis*. Both muscles extend the atlantooccipital joint. *M. rectus capitis ventralis* reaches from the *Arcus ventralis atlantis* to *Pars basilaris ossis occipitalis* and flexes the atlantoocipital joint. *M. longus capitis* also inserts at this part of the occipital bone. *M. rectus capitis lateralis* originates from *Arcus ventralis atlantis* and inserts on *Proc. paracondylaris ossis occipitalis*. Like the other extensors of the atlantooccipital joint, *M. obliquus capitis cranialis* and *M. splenicus capitis* insert on *Squama occipitalis*. The entire *Fossa temporalis* is occupied by the *M. temporalis,* which inserts on the mandibula. (Salomon 2015, Consantinescu 2018, König und Liebich 2005)

The deeper dorsal cervical musculature in the neck region include the cleidocervicals, sterno-occipitalis, sternomastoideus, rhomboideus, splenicus and semispinalis capitis. *M. semispinalis capitis* can be separated into two divisions. The biventer cervicis muscle is the dorsomedial division and reaches from the thoracolumbar fascia and thoracic vertebral transverse processes to the occipital bone. The ventrolateral division is the *M. complexus*, which originates from the cervical vertebral articular processes and inserts lateral to the biventer cervicis muscle on the occipital bone. (Shores and Brisson 2017, Consantinescu 2018)

2.1.3 Anatomy of the brain

The brain can be divided into the telencephalon, diencephalon metencephalon and myelencephalon. The latter two can be summarized as rhombencephalon. The metencephalon includes the cerebellum, which lies dorsally, and the pons. Both parts are connected through *Pedunculi cerebellares medii*. The cerebellum has a hemisphere on each side and a central portion between them, which is called *Vermis*. The cerebellum can also be divided into three lobes that are separated by fissures. *Lobus rostralis* and *Lobus caudalis* are divided by the *Fissura prima*. *Lobus flocculonodularis* lies ventrally to the caudal lobe and is separated by the *Fissura uvulonodularis*. Each lobe consists of a part of vermis and a part of each hemisphere. The lobes are further divided into lobules. The surface of the cerebellum is highly convoluted with folia and sulci or fissures. (Hudson and Hamilton 2010, Constantinescu 2018)

The brain and spinal cord enclose the ventricular system, which is filled with cerebrospinal fluid (CSF). It is composed of four ventricles that are connected with each other through *Foramina interventriculare* (first and second with the third) and *Aqueductus mesencephali* (third with fourth). The fourth ventricle belongs to rhombencephalon. The ventral border is the *Fossa rhomboidea,* which is part of *Pons* and *Medulla oblongata*. Laterally and dorsally, the fourth ventricle lies between the *Pedunculi cerebellares*. Caudally the fourth ventricle continues as the central canal of the spinal cord. (Salomon 2015)

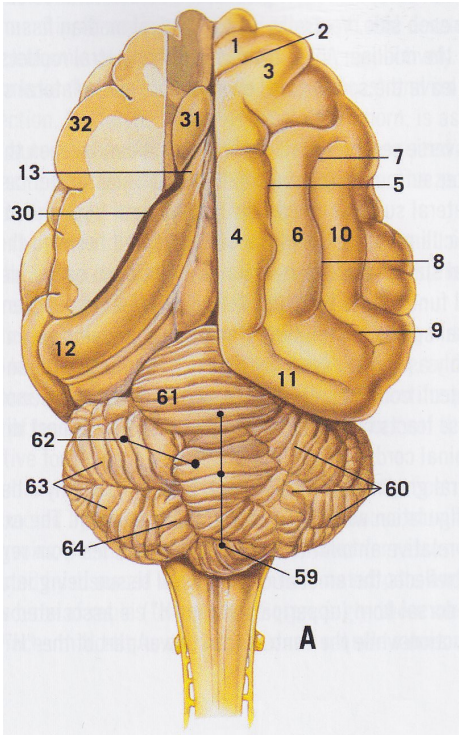

Fig. 3: Brain with portion of left hemisphere removed, dorsal view; 1 Precruciate gyrus 2 Cruciate sulcus 3 Postcruciate gyrus 4 Marginal gyrus 5 Marginal sulcus 6 Ectomarginal gyrus 7 Rostral suprasylvian sulcus 8 Middle suprasylvian sulcus 9 Caudal suprasylvian sulcus 10 Ectosylvian gyrus 11 Occipital gyrus 12 Hippocampal gyrus 13 Fornix 30 Lateral ventricle 31 Caudate nucleus 32 Cerebral cortex 59 Vermis 60 Lateral hemisphere 61 Clumen 62 Declive 63 Ansiform lobule 64 Paramedian lobule (Hudson and Hamilton 2010)

2.1.4 Meninges

In addition to the bony structures of the skull, the brain is protected by three layers of connective tissue, which are called meninges. The outer layer, *Dura mater encephali* is the thickest one. It´s strongly connected to the periosteum of the internal surface of the skull. A number of double folds of dura mater exist. The most important ones being *Falx cerebri*, *Tentorium cerebelli membranaceum* and *Diaphragma sellae*. The tentorium is located in the transverse fissures between the cerebellum and cerebrum. Profoundly to the *Dura mater* lies the *Arachnoidea enchephali* and the *Pia mater encephali*, which together create the *Leptomeninx*. Meningiomas are intercranial neoplasia originating from the meninges. (Hudson and Hamilton 2010)

2.1.5 Vessels of the brain

The main arterial supply to the head comes from the left and right common carotid arteries. The vertebral artery also contributes blood to the occipital and cerebral circulation. On the base of the brain lies an arterial circle, called circle of Willis. In contrast to most other mammals the feline internal carotid artery does not supply the circle of Willis, as it degenerates postnatal. Instead, multiple branches from the maxillary artery, which is a branch from the external carotid artery, form a rete mirabile maxillaris. Several *Rami retis* leave this network and enter the arterial circle. The arterial circle is further formed by the caudal communicating arteries and the basilar artery. A number of arteries, such as the rostral, middle and caudal cerebral arteries, leave the circle of Willis to supply large areas of brain parenchyma. The rostral cerebellar arteries also branch off the arterial circle. The caudal cerebellar arteries and the pontine arteries, which supply the metencephalon, usually branch off the basilar artery caudal to the arterial circle. The occipital artery branches off the external carotid artery and extends dorsally to supply the neck and the occipital region. (Hudson and Hamilton 2010, Constantinescu 2018)

A system of *Sinus durae matris* carry the venous blood from the brain. The vessels do not satellite the arteries but lie independently in a complex structure. The dorsal sagittal sinus collects blood from the dorsal aspects of the cerebrum. It runs in the midline along the *Falx cerebri*. Near the caudal end it joins with the straight sinus, which is also on the midline but at a deeper level. At the caudal end the dorsal sagittal sinus enters a foramen that divides into the bilateral transverse sinus. The left and right transverse sinus travel laterally within the *Tentorium cerebelli*, which is part of the occipital bone. They are connected with each other through the *Sinus communicans*. Ventrally to the *Protuberantia occipitalis interna* lies the *Confluens sinuum*, which is an asymetrical void that carries blood from the dorsal sagittal sinus, the straight sinus and the occipital sinus. Ventrally the transverse sinuses join the cavernous sinus, which is part of the ventral sinus. The continuation of the transverse sinus together with the *Vena (V.) emissaria foraminis jugularis*, is called *Sinus sigmoideus*. The ventral sinus collects blood from the ventral brain areas. *Plexus opthalmicus*, which lies within the orbita is connected with the cavernous sinus through the *Venae (Vv.) emissaria fissurae orbitalis*. Caudally the cavernous sinus continues as the ventral petrosal sinus. It then continues as the basilar sinus, which leaves the skull through the *For. magnum* and joins the venous network in the spinal canal. (Hudson and Hamilton 2010, Salomon 2015, Constantinescu 2018)

Multiple *Vv. emissariae* create connections between the sinus system and the veins of the skull. The *V. emissaria mastoidea* leaves the sigmoid sinus and perforates the skull through

the *For. mastoideum*. The occipital emissary vein leaves the transverse sinus, perforates the occipital bone near the nuchal crest and joins the mastoid emissary vein. (Constantinescu 2018)

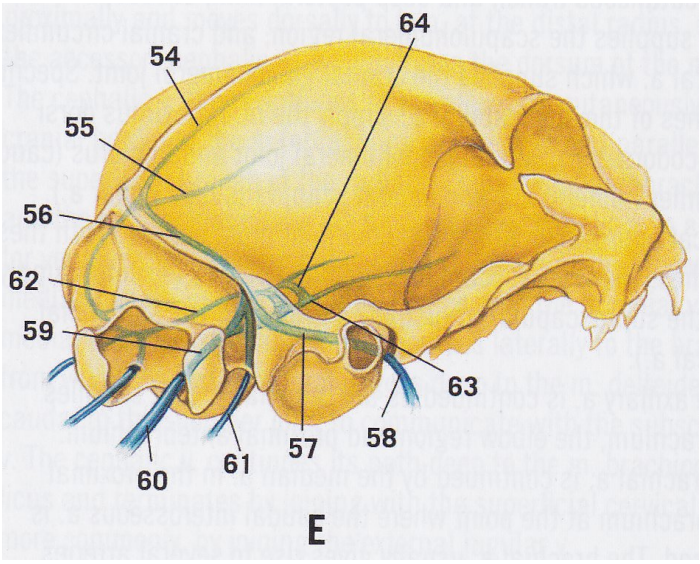

Fig. 4: Major venous sinuses of brain, caudolateral view; 54 Dorsal sagittal sinus 55 Straight sinus 56 Transverse sinus 57 Temporal sinus 58 Retroarticular vein 59 Condyloid vein 60 Basilar sinus 61 Internal jugular vein 62 Ventral petrosal sinus 63 Cavernous sinus 64 Intercavernous sinus (Hudson and Hamilton 2010)

2.2 Meningioma in cats

One of the most common indications for brain surgery in cats is tumor removal. The most frequently found primary tumor is meningioma. (Troxel et al 2003)

Meningioma are mesenchymal brain tumors that typically arise from the arachnoid, but also the dura mater or pia mater. Most commonly feline meningioma are solitary, even though cases with multiple ones have been reported. They are usually located over the cerebral hemisphere but can also be found in other regions. Due to the slow growth, meningioma are associated with an insidious onset of clinical signs, which often start with behavioral changes. Diagnosis can be confirmed with MRI, as meningioma are typically seen as hyperintense mass lesions on T1-weighted pre- and postcontrast sequences. Dural tail sign is another typical appearance of meningioma.

Solitary meningioma can often be successfully treated with surgical removal. Many studies show a good to excellent long-term survival. A study from Cameron et al. showed a low perioperative mortality of 6 % and a median survival of 38 months for survivors of the perioperative phase. In contrast, the surgical removal of other intracranial neoplasia is associated with a much higher mortality. (Langley-Hobbs et al. 2014, Cameron et al. 2015)

2.3 Suboccipital craniotomy in small animals

Suboccipital craniotomy is fairly often performed in dogs with Chiari-like malformation, in order to establish foramen magnum decompression. For this procedure, it can be necessary to extend the approach caudally by partial or complete removal of the dorsal arch of the atlas. For other indications like tumor excision usually only part of the occipital bone is removed. (Fossum 2019)

The transverse sinus is an important vascular structure that should be avoided during craniotomy. A laceration of this vessel can cause life-threatening hemorrhage. Ligation or obstruction of both transverse sinuses or the confluens sinus is likely to end in massive brain swelling, which can also be fatal. Nevertheless a permanent occlusion of the transverse sinus, as described in 2.3.4 and 2.5, is possible. It is also common to come across bleeding from the occipital emissary veins. This can be controlled by pushing bone wax into the mastoid foramen, which is where the vein exits the skull. (Fossum 2019)

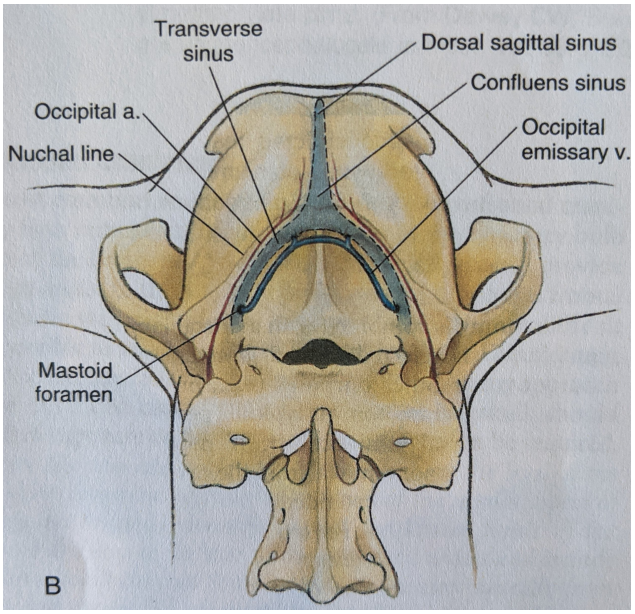

Fig. 5: Illustration of the canine skull with important vascular structures (Fossum 2019)

2.3.1 Surgical approach

The patient is positioned in sternal recumbency with a ventroflexed head. The positioning is secured with surgical tape, sandbags or a head restraint device. Vacuum cushions can also be used. (Langley-Hobbs et al. 2014) The area from the level of the bregma to the level of the third or fourth cervical vertebra is clipped and aseptically prepared. A dorsal midline incision is made. It should extend from 1-2 cm rostral to the external occipital protuberance to the caudal aspect of the spinous process of the second cervical vertebra. After the subcutaneous tissue is incised in the midline and retracted, the superficial cervical muscles

are exposed. These are incised along the median raphe until the deeper cervical muscles are visible. The dissection continues in the midline through the biventer cervicis muscles and *Rectus capitis dorsalis*. The surgeon now elevates the musculature from the occipital bone using a Freer periostal elevator. Hemorrhage is controlled with monopolar or bipolar electrocautery.

In dogs with extensive occipital dysplasia, mainly in smaller breeds, it is important to carefully evaluate the structure of the occipital bone before periosteal elevation of the muscles. In these patients only a thin periosteal membrane protects the cerebellum or the muscle directly overlies the dura membrane.

After Gelpi or other self-retaining retractors are placed, it is controlled if adequate exposure was achieved. For the removal of an intracranial tumor, the dissection extends to the following structures: laterally and dorsally the nuchal crest and occipital protuberance, ventrolaterally the occipital condyles and ventrocaudally the foramen magnum.

After the exposure is completed, the craniotomy or craniectomy is performed. Due to the thinness of the occipital bone in dogs with severe occipital dysplasia, craniectomy can be performed with only the use of Kerrison and Lempert rongeurs. In thicker bones a high power nitrogen drill is used to make one or more burr-holes lateral to the midline. The opening is expanded using Kerrison and Lempert rongeurs.

The bony defect can extend from just ventral to the nuchal crest laterally and just ventral to the occipital protuberance dorsally and to the foramen magnum ventrally. The ventrolateral borders are the occipital condyles. Staying within these boundaries, protects the dorsal sagittal sinus, confluens sinuum and the transverse sinus. If the dissection is continued to far ventrolaterally, the condylar vein, which drains the sigmoid sinus, can be lacerated. The extent of the bony defect is tailored to the given indication and can vary in size and shape. (Shores and Brisson 2017)

If it is necessary to extend the suboccipital craniotomy laterally, one of the transverse sinuses can be sacrificed. If more room is needed caudally, the surgeon can remove parts or the complete dorsal arch of the atlas. (Fossum 2019)

After the demanded portion of the occiput is removed and possible hemorrhage is under control, the tissues are lavaged with saline. Afterwards the exposed meninges are incised longitudinally using a number twelve scalpel blade. The initial opening is expanded rostrally and caudally with the use of Potts-Smith or tenotomy scissors. If the desired length is achieved the rostral and caudal end is expanded laterally, so that the incision becomes the

shape of the letter H. The surgeon can apply stay sutures before or after the incision to maintain retraction of the meninges.

The remaining steps depend on the initial indication for surgery. Tissues of the nervous system must always be handled with great care. The use of lint-free cellulose spears can help to preserve the delicate brain parenchyma. (Shores and Brisson 2017)

After the meninges are opened and the brain is exposed, it is important, that the surgery is continued time-efficient. Prolonged exposure of brain tissue is associated with increased postoperative morbidity, even if the tissues are kept moist with saline and sponges. (Fossum 2019)

2.3.2 Tumor removal

Meningiomas usually arise from the dura mater itself. In that case, a circumferential incision removing the dura and tumor together needs to be made. In gliomas the dura can be incised as previously described and later used for closure. The margins of peripheral brain tumors are carefully explored using neurosurgical probes. Small vessels leading to the tumor can be cauterized with bipolar electrocautery. Thrombin gel foam helps to control diffuse hemorrhage. A suction device is used to remove neoplastic tissue and can also be used as a dull dissector between tumor and healthy brain tissue. Any suction device needs to be handled with care as brain parenchyma is easily damaged.

The surgeon can differentiate between tumor and normal brain tissue based on consistency, abnormal color or available imaging during surgery. Meningiomas usually have firmer consistency and a sharp border towards the normal brain parenchyma. The tumor may even roll out of the calvarium. (Langley-Hobbs et al. 2014)

2.3.3 Closure of the surgical field

A significant impression on the brain tissue may be left after tumor removal. This cavity can be filled with thrombin gel foam. Most often it is not necessary to replace the bone flap. In extensive craniotomies using a gamma-irradiated calvarial allograft or other reconstruction methods have been described. When the dura mater can be closed a fascial transplant from the temporal muscle can be used to close the brain cavity. After closure of the meninges, the temporal muscle is placed over the bony defect and re-attached to its insertion on the midline. The skin closure is proceeded as usual. (Langley-Hobbs et al. 2014)

2.3.4 Rostrolateral extension of the suboccipital craniotomy approach

The suboccipital approach, executed as previously described, enables only limited exposure of the dorsal and rostral portions of the cerebellum and the cerebellopontine angle. To ensure better access to the caudal fossa, the suboccipital approach can be combined with a rostrotentorial approach. This rostrolateral extension of the bony defect entails the occlusion of the transverse sinus. After skin incision and elevation of the temporal muscles, a drill is used to remove the bone surrounding the sinus until it is visible. Care is necessary to keep the thin sinus wall intact. After the transverse sinus is exposed, it can be ligated with the use of bipolar electrosurgical cautery. The sinus can also be occluded with the use of bone wax or gelatin foam into the bony canal and groove, respectively, surrounding the transverse sinus. (Johnston and Tobias 2018)

As sinus ligation is associated with a greater surgical risk and the most significant obstacle in successful execution of a combined rostrotentorial and suboccipital approach, the subject will be further discussed in chapter 1.5. (Maiuri et al. 2019, Pluhar et al. 1996)

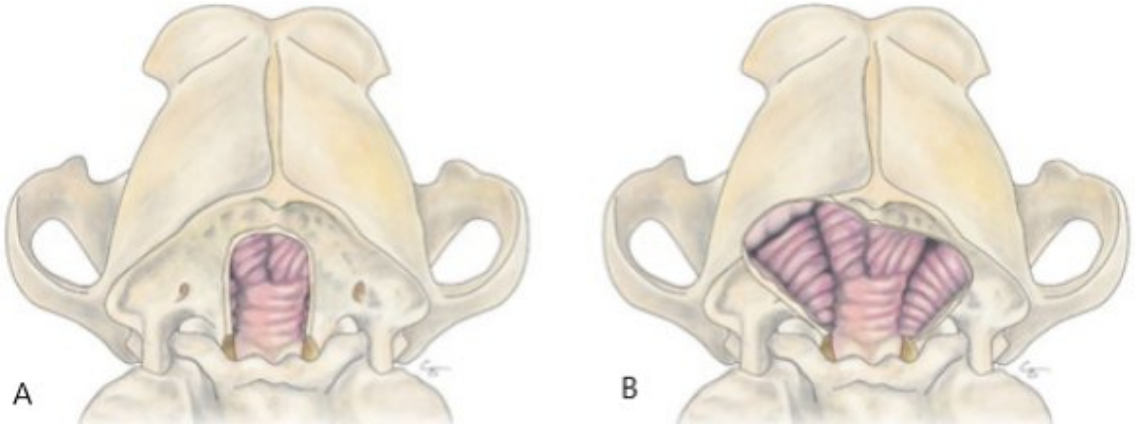

Fig. 6: Illustration of the approaches to the caudal fossa of the canine skull, A) standard suboccipital approach, often used for the treatment of Chiari-like malformation, B) combined suboccipital and rostrotentorial approach (Johnston and Tobias 2018)

2.4 Suboccipital craniotomy in human medicine

As most surgical techniques in veterinary medicine are based on those used in human beings, this chapter will give an overview of surgical approaches for the suboccipital region in human medicine.

Surgical approaches in this region are also often referred to as retrosigmoid approach or posterior fossa craniotomy. (Greenberg 2016)

2.4.1 Midline occipital approach

This approach is commonly used to treat lesions in the midline of the posterior fossa. Similarly, to suboccipital craniotomy in dogs, it can also be used for decompression in human patients with Chiari malformation. A midline skin incision is made appropriate to the size of the tumor. After the muscles are displaced a craniotomy or craniectomy is performed. Several burr holes are placed in the midline or paramidline. Afterwards a craniotome or rongeur is used to connect the drill holes and created the craniotomy window, which usually extends inferior to the *For. magnum*. A laminectomy of the first cervical vertebra is helpful to maximize access to the *For. magnum* and neighboring structures.(Di Ieva et al, 2016, Greenberg 2016)

2.4.2 Paramedian suboccipital craniectomy

Among other indications this approach is used to access the cerebellopontine angle or lesions concerning one hemisphere. For small tumors a linear skin incision 5 mm medial to the mastoid notch can be made. If larger access is necessary the surgeon can use a so-called hockey-stick incision, extending in a curved shape from the spinous process of the second cervical vertebra to the inion and then the mastiod process.

The craniotomy window is limited superiorly by the transverse sinus, inferiorly by the *For. magnum* and laterally by the sigmoid sinus. Usually it only reaches to the midline medially, but extension in this direction is possible. For smaller lesions, it might be sufficient to place a round window with a diameter of two to four centimeters in the angle created by the transverse and sigmoid sinus. (Greenberg 2016)

2.4.3 Far lateral approach

For this approach a hockey-stick skin incision, starting from the spinous process of the second cervical vertebra to just behind the external acoustic meatus, is usual. The craniotomy window extends to the transverse sinus superiorly and the *For. magnum* inferiorly. Laterally the bony defect is limited by the occipital condyle. Depending on the size and location of the lesion, the medial occipital condyle can be partly removed. (Di Ieva et al 2016)

2.4.4 Extended retrosigmoid approach

This approach is a combination between the far lateral and the retrosigmoid approach. The skin incision is shaped like a C and is positioned behind the ear. The muscles can also be incised C-shaped, creating a musculocutaneous flap that can be retracted anteriorly. Afterwards a mastoidectomy and skeletonization of the sigmoid sinus are carried out. A craniotomy window is created, reaching from the transverse sinus superiorly to approximately 5 cm behind the sigmoid posteriorly. (Sekhar and Fessler 2016)

2.5 Transverse sinus occlusion in human and veterinary medicine

In order to complete a combined rostrotentroial and suboccipital approach the occlusion of the transverse sinus is necessary. The extended craniotomy window and the obliteration of the transverse sinus, respectively, significantly improve the accessibility of the cerebellum, the ipsilateral cerebellopontine angle and the ipsilateral brain stem. (Pulhar et al 1996)

On the downside, occlusion of the transverse sinus is associated with the possibility of a sudden rise in intracranial pressure (ICP), following acute brain swelling and death. (Oliver JE 1968). On the contrary, an experimental study by Pluhar et al. showed that in their subject group of six healthy dogs an unilateral transverse sinus occlusion did not lead to a rise in ICP. Another study by Bagley et al. detected no increase in ICP after the ligation of the transverse sinus in five dogs with an intracranial mass. After the craniotomy window was established and the dura mater was incised, the ICP even decreased. Therefore, a craniectomy helps to manage cerebral edema during surgery and post operatively. Furthermore, it is vital to keep the associated cortical veins intact. (Bagley et al. 1997, Pluhar et al. 1996)

In human medicine, sinus occlusion is also associated with the risk of venous infarction. To lower the risk of complications during surgery a MR angiography can be run to determine the circulation pattern. In some patients, venous sinus drainage is not equal on both sides. The ligation of the transverse sinus is only recommended if the concerned side is non dominant. Another method to lower the risk of potential brain swelling, is to test clamp the transverse sinus during surgery and wait a couple of minutes if acute edema occurs. If it does, the clamp should be removed, reestablishing venous drainage. If no rise in the ICP is detectable, the sinus can be permanently occluded. (Maiuri et al 2019)

3 Materials and Methods

In order to execute a virtual craniotomy, diagnostic images (CT and MRI scans) of the head of seven cats were used retrospectively. The data was collected from the Clinical Unit of Diagnostic Imaging of the University of Veterinary Medicine Vienna. None of the cats received the CT and MRI scans due to brain pathologies. The shape of the skull was not a criteria for exclusion and the subjects were not divided into a mesocephalic and brachycephalic group.

All following steps were carried out with the Amira® computer program and the help of Dr. Stephan Handschuh, part of the VetCore Facility for Research at the University of Veterinary Medicine Vienna. First, the CT and MRI files were converted from a DICOM to an AMIRA format. A 3D model of the CT file was created using the isosurface tool with a threshold set over 350 Hounsfield Units, so only the bones of the skull were visible. The cervical vertebrae were removed to achieve better access to the occipital bone. The CT and MR images were laid over each other and the brain was extracted by hand. Therewith a 3D model of the brain, that aligned with the cranial bones, was created.

The previously constructed models of the brain and the skull were then used to carry out three different suboccipital craniotomy approaches. The first one was a standard approach as described in the literature. (Fossum 2019, Shores and Brisson 2017) The second and third were rostrally extended to the left or right, additionally impacting the parietal bone, which would cause a transverse sinus occlusion in real life. In the tables of this thesis the standard approach is referred to as App 1 and the extended approaches are referred to as App 2 left and App 2 right.

3.1 Measurement the surface of the cerebellum and its compartments

The previously created surface file was visualized with a surface view and the surface editor was activated. The surface of the brain now consisted of small triangles. A tool called “draw contour to highlight faces” was used to mark all triangles within the wanted area. The MRI sequence was also visualized as a Volren display overlaying the surface view, which helped to identify the different brain structures and find the right borders. After the correct area was marked a new Boundary ID was set, which applied a specific color and name to the area, as listed in Tab. 1. Afterwards the area was cleared, so the next area could be marked. This procedure was carried out for the surface of the cerebellum of all seven cats. Afterwards the same process was completed for the different compartments of the cerebellum - the vermis, the left and the right hemisphere, always in this order. It was important, that the highlighted

areas did not overlap each other, as the intersection would be calculated as an additional area. The surface with the three marked regions was saved as a separate file. Part of the cranial region of the cerebellum is physiologically covered by the left and right hemisphere of the cerebrum. In order to measure the whole surface of the cerebellum, a segment of the caudal cerebrum was extracted, making the cranial region of the cerebellum visible. All newly created files were saved separately as surface files with the according Boundary IDs.

In the next step a tool called “Surface Area Volume” was used to calculate the number of square millimeters of each of the previously marked areas or Boundary IDs respectively. The results were listed as cerebellum surface, cerebellum whole surface, vermis, left hemisphere and right hemisphere.

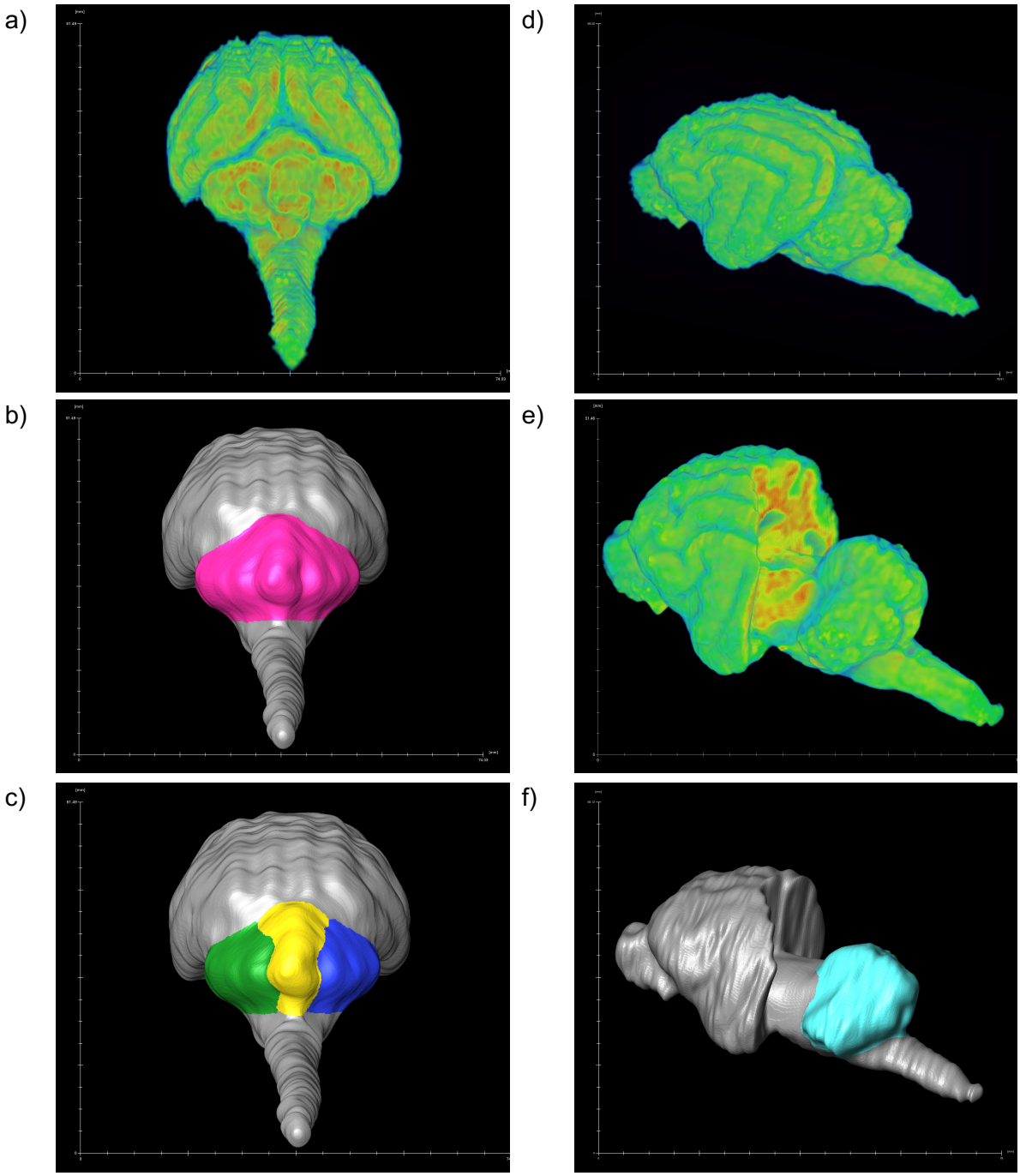

Fig. 7: caudodorsal and lateral view of a 3D reconstruction of MRI scans of the brain of cat 3 and 5
a) visualized as volren image
b) surface view, with the cerebellum highlighted
c) surface view with highlighted cerebellar compartments , vermis (yellow), left (green) and right hemisphere (blue)
d) visualized as a volren image in lateral view
e) volren image with extraction of a caudal portion of the cerebrum, rostral part of the cerebellum visible
f) surface view of brain with extracted caudal segment of the cerebrum and the whole cerebellar surface highlighted

3.2 Measurement of the occipital bone

Using the CT volume an Isosurface with a threshold at 350 Hounsfield Units was generated. This display only shows the cranial bones as a 3D model. Similarly to the measurement of the surface of the cerebellum in 3.1, the surface editor was activated and the surface of the entire occipital bone was highlighted. Afterwards a new Boundry ID with a specific color was set (Tab. 1) and the number of square millimeters was calculated using the Surface Area Volume tool. The new data was saved separately as a surface file.

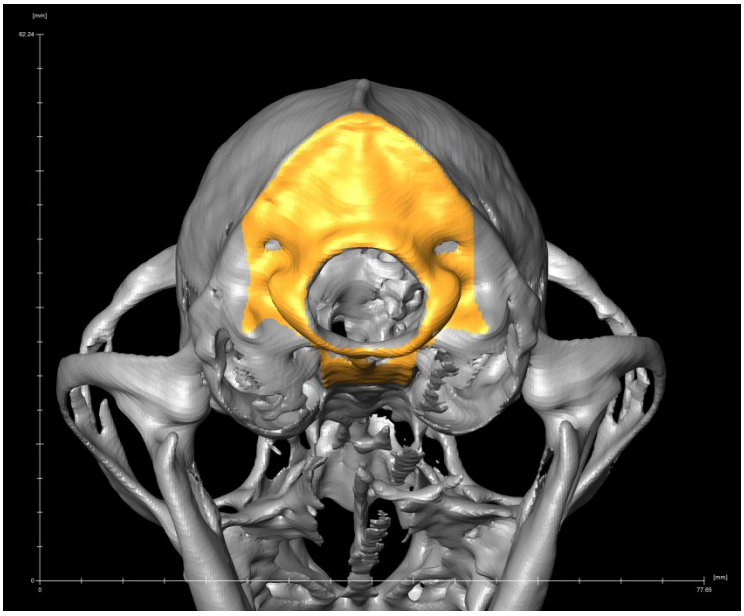

Fig. 8: occipital bone highlighted on a 3D reconstruction of CT scans of a skull without the cervical spine of a cat, visualized with surface view

Tab. 1: Colors of the measured areas

area	color	settings identifying the color using the HSV color model
cerebellum surface	pink	0.900 - 0.800 - 1.000
cerebellum whole surface	turquoise	0.500 - 0.600 - 1.000
vermis	yellow	0.150 - 0.900 - 0.950
left hemisphere	green	0.350 - 0.800 - 0.600
right hemisphere	blue	0.650 - 0.800 - 1.000
occipital bone surface	orange	0.100 - 0.800 - 1.000

3.3 Placement of the drill holes

With a tool called landmark editor, three to five landmarks were set, imitating the drill holes of a craniotomy approach. For the standard approach three landmarks were placed at the following locations:

a. in the midline at approximately 85 % of the distance dorsal edge of the *Foramen magnum* to the *Protuberantia occipitalis*

b. just ventrally the *Crista nuchae* at the level of the middle of the occipital condyle on the left side

c. same as b. on the right side

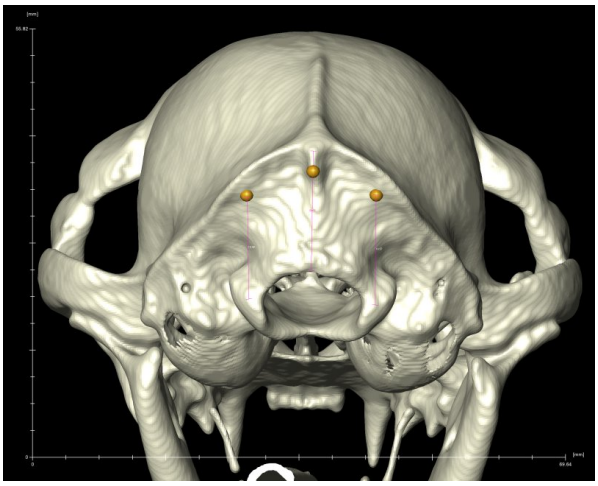

Fig. 9: Placement of the landmarks representing the drill holes of the standard approach

For the rostrally extended approaches to the left and the right side, two additional landmarks were place at the following locations on each side:

a. 5 mm lateral to the rostral end of the *Crista saggitalis*

b. 1 cm dorsal to the caudal edge of *Processus mastoideus*

The landmarks were placed with the assistance of a measuring tool. The newly created data was saved as a landmark file for each of the approaches.

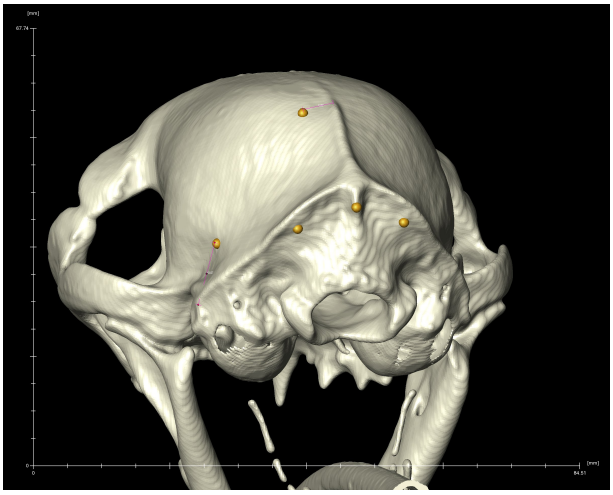

Fig. 10: Placement of the landmarks representing the drillholes of the extended approach to the left

Fig. 11: Placement of the landmarks for the extended approach to the left, lateral view

3.4 Measurement of the craniotomy window

The surface model of the CT scans was used again to measure the area that will later be cut out, creating a craniotomy window. For this purpose the surface editor was activated and the landmark file, that was created beforehand, was opened. For the standard approach the landmarks a., b. and c. were connected using a drawing tool. The area between those lines and the Foramen magnum was then marked and set as a new Boundary ID. For the extended approaches the landmarks d. and e. on the according side were connected with each other and the borders of the previously marked area that visualizes the standard approach. For each side a new Boundary ID was set and saved as a separate file. Afterwards the Surface Area Volume tool was used to calculate the number of square millimeters of each of the areas. The area of each of the extended approaches was then added to the standard approach to represent the whole area of the extended approach, as it would be in real life.

Tab. 2: Colors of the measured areas of the craniotomy windows

area	color	settings identifying the color using the HSV color model
Craniotomy window App 1	dark purple	0.720 - 0.870 - 0.840
Craniotomy window App 2 left	custom purple	0.667 - 0.502 - 1.000
Craniotomy window App 2 right	custom purple	0.667 - 0.502 - 1.000

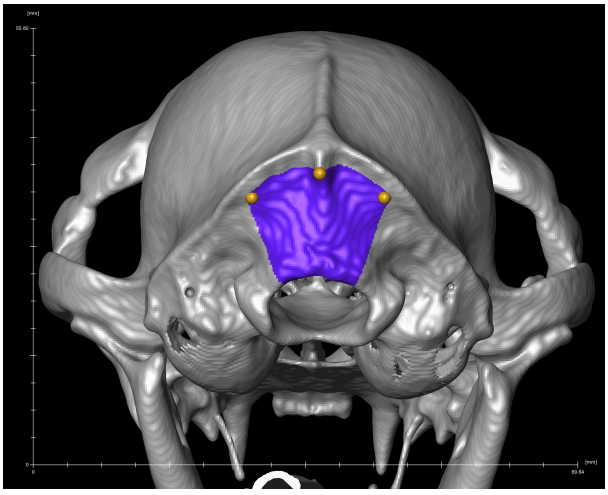

Fig. 12: Area representing the craniotomy window for the standard approach with associated landmarks

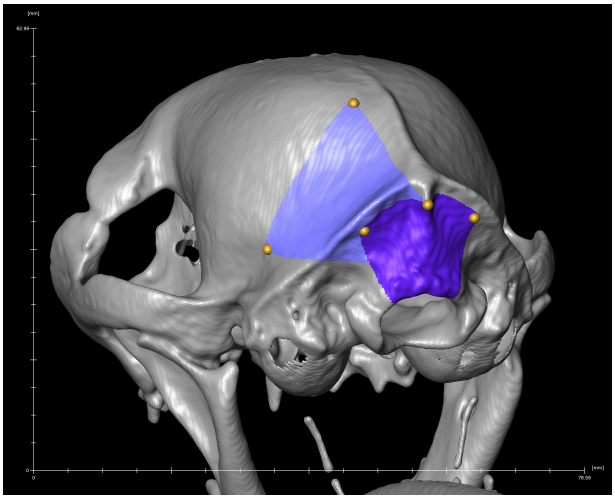

Fig. 13: Area representing the cranial extension to the left (light purple) and area representing the standard approach (dark purple), together representing the extended approach to the left, with associated landmarks

3.5 Cutting of the craniotomy window

After the measurement of the craniotomy windows as described in 3.4, the surface editor was activated again. The option “visible triangles only” is deactivated, which had the effect of highlighting not only the triangles on the surface but also on the backside and all in between. All marked triangles outside the wanted area were removed again. Afterwards the feature “delete highlighted surfaces” is applied, which creates an opening corresponding to a craniotomy window in real life. This work flow was repeated for all three craniotomy approaches.

3.6 Measurement of areas through the craniotomy window

The surface file of the skull containing the craniotomy window was opened and made visible with the surface view tool. The surface file created as described in 3.1, with the highlighted surface of the cerebellum and its compartments respectively, was also opened. For the latter the surface editor was activated. In order to meet the right angles, the view was changed from perspective to orthographic. Thereafter the area visible through the bony defect was highlighted. A new Boundary ID, overlaying the other Boundary IDs, was set. All Boundary IDs that were created in this step were assigned the color custom red (color setting at 0.0 – 0.891 – 0.863). Afterwards the tool “Surface Area Volume” was used to generate an analyzing file. This file showed a table of the measured or calculated areas in square millimeters in the same order as listed in Tab. 3. Overflow represents the area of the brain surface, that is not assigned a Boundary ID.

Tab. 3: Order of the measured areas in the analyzing file described in 3.6

#	cerebellum surface	cerebellum compartments
1	overflow not visible	overflow not visible
2	cerebellum not visible	vermis not visible
3	overflow visible	left hemisphere not visible
4	cerebellum visible	right hemisphere not visible
5		overflow visible
6		vermis visible
7		left hemisphere visible
8		right hemisphere visible

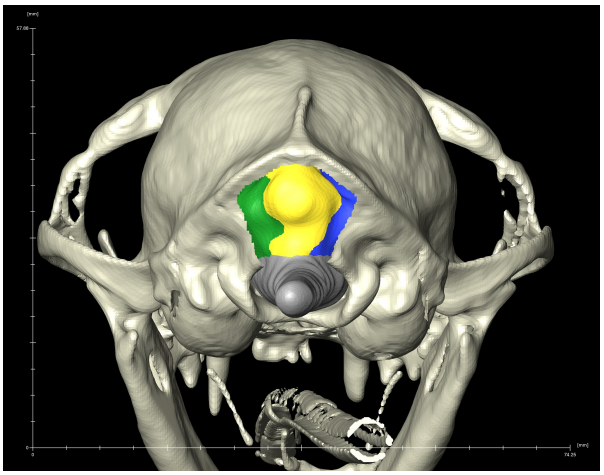

Fig. 14: Craniotomy window of the standard approach, with part of the underlying cerebellar compartments visible

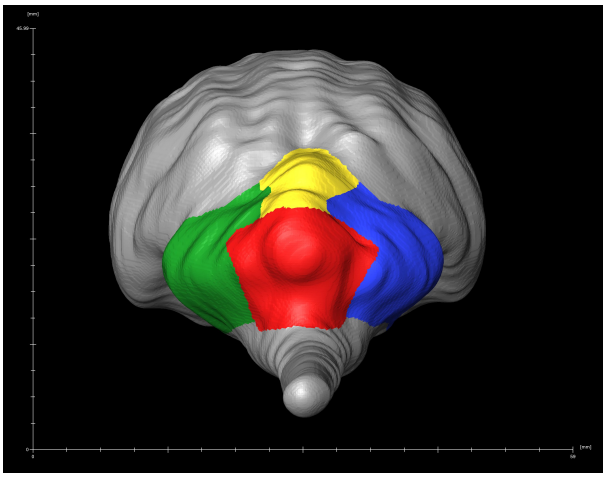

Fig. 15: Cerebellum with compartments, area that is visible through the craniotomy window of the standard approach is marked red

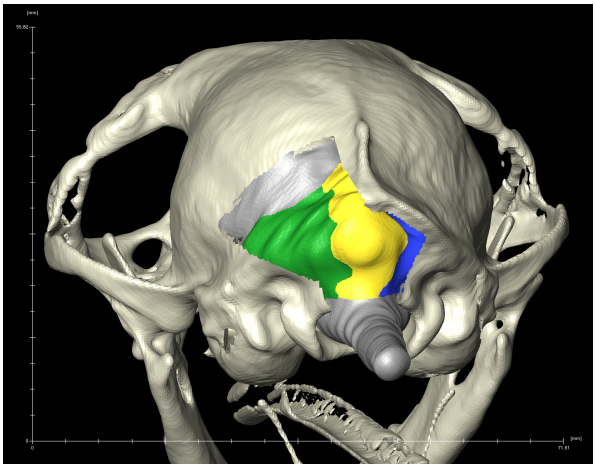

Fig. 16: Craniotomy window of the extended approach to the left, with part of the underlying cerebellar compartments visible

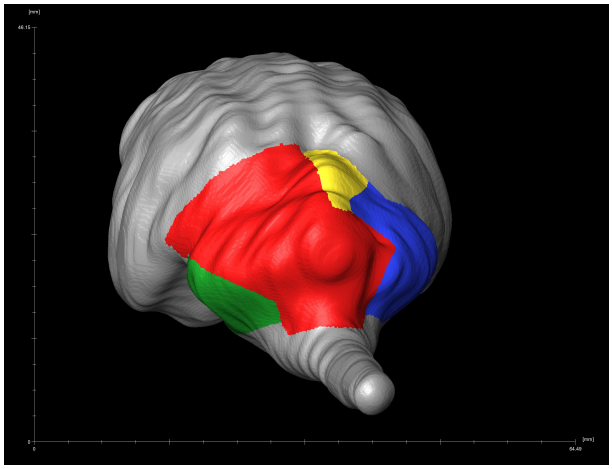

Fig. 17: Cerebellum with compartments, area that is visible through the craniotomy window of the extended approach to the left is marked red

3.7 Statistics

For this thesis descriptive statistics were used to evaluate the collected data. The average value and standard deviation of the subject group was calculated for all measured areas described in 3.1, 3.2, 3.4 and 3.6. All results given in square millimeters and in percentage were rounded to one decimal place. Furthermore the following parameters were determined. For those parameters the average and standard deviation of the subject group was also evaluated. All parameters concerning the cerebellum, except the values q, r and s, were calculated using the area of the cerebellar surface with the cerebrum in situ.

3.7.1 Percentage of removed bone in the standard approach (b)

b = removed bone : occipital bone * 100

3.7.2 Percentage of Vermis visible in the different approaches (e, f, g)

For App 1	e = vermis visible : vermis * 100
For App 2 left	f = vermis visible : vermis * 100
For App 2 right	g = vermis visible : vermis * 100

3.7.3 Percentage of left hemisphere visible through the different approaches (h, i, j)

For App 1	h = left hemisphere visible : left hemisphere * 100
For App 2 left	i = left hemisphere visible : left hemisphere * 100
For App 2 right	g = left hemisphere visible : left hemisphere * 100

3.7.4 Percentage of right hemisphere through the different approaches (k, l, m)

For App 1	k = left hemisphere visible : left hemisphere * 100
For App 2 left	l = left hemisphere visible : left hemisphere * 100
For App 2 right	m = left hemisphere visible : left hemisphere * 100

3.7.5 Percentage of cerebellum through the different approaches (n, o, p)

For App 1	n = cerebellum visible : cerebellum * 100
For App 2 left	o = cerebellum visible : cerebellum * 100
For App 2 right	p = cerebellum visible : cerebellum * 100

3.7.6 Percentage of accessed cerebellum compared to the whole surface of the cerebellum in all approaches (q, r, s)

For App 1	q = cerebellum visible : cerebellum whole surface * 100
For App 2 left	r = cerebellum visible : cerebellum whole surface * 100
For App 2 right	s = cerebellum visible : cerebellum whole surface * 100

3.7.7 Percentage increase in access in the extended approach to the left compared to the standard approach (t, u, v)

For the vermis	t = 100 * (f - e) / e
For the left hemisphere	u = 100 * (l - h) / h
For the right hemisphere	v = 100 * (l - k) / k

3.7.8 Percentage increase in access in the extended approach to the right compared to the standard approach (w, x, y)

For the vermis	w = 100 * (g - e) / e
For the left hemisphere	x = 100 * (j - h) / h
For the right hemisphere	y = 100 * (m - k)

4 Results

Three different kinds of craniotomy approaches were virtually carried out. The first one was a maximized version of the standard approach, as it is described in the literature. (Fossum 2019, Shores and Brisson 2017) The second and third one were rostrally extended to the left and right side, additionally impacting the parietal bone.

Even though the measurements of the seven cats differ from each other to a small extent, they show the same pattern and can be compared to each other (Fig. 18, Fig. 19). There were no apparent outliers, so the data of all seven cats was used for calculation and interpretation.

4.1 Landmarks that represent the drill holes

In order to maximize the accessibility of the standard approach, the landmarks that represent the drill holes were placed as dorsal as possible, without endangering the transverse sinus and the confluens sinuum. The first one was placed in the midline at approximately 85% of the distance dorsal edge of the *Foramen magnum* to the *Protuberantia occipitalis.* The second and third one just ventrally the *Crista nuchae* at the level of the middle of the occipital condyle on the left and right side.

For the extended approaches to the left and right two additional drill holes were set on each side. To guarantee accurate comparison between the seven cats, the position of the drill holes were described using anatomical landmarks, that are also palpable in real life. The first additional drill hole was placed 5 mm lateral to the rostral end of the *Crista sagittalis* on the appropriate side. The second set of drill holes was placed 1 cm dorsal to the caudal edge of the *Processus mastoideus* on each side.

4.2 Measured surfaces of the brain

The areas of the brain surface were manually marked and measured in mm² as they are listed in Tab. 4. The whole surface of the cerebellum was marked on the surface file with the previously extracted segment of the caudal cerebrum. On average, the area was 1127.7 mm². The mean value of the cerebellar surface was 836.9 mm² (SD: 59.8 mm²); meaning that only about 70 % of the cerebellar surface is visible with the cerebrum intact. The cerebellar surface was further divided into the vermis, with a mean value of 210.0 mm² (SD: 29.5 mm²) and two hemispheres. On average the right hemisphere, with a mean value of 317.4 mm² (SD: 29.4 mm²) was slightly bigger than the left hemisphere, with a mean value of 307.7 mm² (SD: 20.8 mm²). For all further calculations concerning the cerebellum the

value of the cerebellar surface with the cerebrum in situ (Tab. 4, third column) was used as a reference.

Tab. 4: Measured surfaces of the different areas of the brain in mm²

	Cerebellum whole surface	Cerebellum	Vermis	Hemi-sphere left	Hemi-sphere right
Cat 1	1146.2	811.0	210.7	298.0	303.0
Cat 2	1148.4	847.2	198.9	314.7	332.4
Cat 3	1056.3	845.3	224.9	309.2	306.8
Cat 4	989.2	720.4	159.1	282.9	275.1
Cat 5	1172.8	905.3	198.2	343.5	361.4
Cat 6	1234.2	885.1	254.3	286.9	342.4
Cat 7	1147.0	843.8	223.7	318.5	300.6
Average (MV)	1127.7	836.9	210.0	307.7	317.4
Standard deviation (SD)	80.4	59.8	29.5	20.8	29.4

4.3 Measured surfaces of the cranial bones and craniotomy windows

The following measurements were carried out on the 3D model of the CT scans. All measurements are listed in Tab. 5. The measurements of the occipital bone were quite different from cat to cat. The mean value was 1032.7 mm² and the standard deviation 152.6 mm². The craniotomy window of the standard approach was bounded by the landmarks a., b. and c., as described in 3.3, and the For. magnum. The mean value was 272.9 mm² (SD: 67.5 mm²). In order to measure the craniotomy window of the extended approaches the area between the landmarks d. and e., as described in 3.3, and the borders of the standard approach was marked. This area was 375.9 mm² (SD: 107.5 mm²) on average for the left side and 384.8 mm² (SD: 73.3 mm²) on average for the right side. Afterwards the measured area was added to the standard approach, which corresponds to the area of the craniotomy window that was later cut. The entire craniotomy window of the extended approach to the left was 648.8 mm² (SD: 165.7 mm²) big. The one on the right side was slightly bigger, with a mean value of 657.7 mm² (SD: 113.2 mm²).

Tab. 5: Measured surface of the occipital bone and the areas of the craniotomy windows in mm²

	Occiput surface	Craniotomy window App 1	Craniotomy window App 2 left	App1 +App2 left	Craniotomy window App 2 right	App1 +App2 right
Cat 1	1257.0	241.9	281.3	523.3	376.4	618.3
Cat 2	1063.5	393.3	482.6	875.9	440.2	833.5
Cat 3	926.4	204.5	325.2	529.8	339.7	544.3
Cat 4	917.3	278.7	310.0	588.7	342.0	620.7
Cat 5	888.9	226.2	342.2	568.4	509.0	735.2
Cat 6	1223.9	331.7	570.3	902.0	399.5	731.2
Cat 7	951.7	234.1	319.6	553.8	286.7	520.8
MV	1032.7	272.9	375.9	648.8	384.8	657.7
SD	152.6	67.5	107.5	165.7	73.3	113.2

4.4 Visible and non-visible areas through the standard approach

The brain surface files were overlaid with the CT files, where the craniotomy window for the standard approach was previously cut. The areas of the cerebellum visible through the created bony defect were marked and the measurements listed in table 6 and 7. On average 205.7 mm² (SD: 24.6 mm²)of the cerebellum were visible, leaving 631.2 mm² (SD: 55.4 mm²) not visible. The non visible area is related to the cerebellar surface with the cerebrum in place and not the whole cerebellar surface. The overflow area represents the surface visible through the craniotomy window, that was not assigned to a Boundary ID. In this approach it mostly consists of parts of the Medulla oblongata.

Furthermore, the surface file with the cerebellar compartments was used in the same way. On average 112.9 mm² (SD: 21.0 mm²) of the vermis were visible and 97.1 mm² (SD: 16.9 mm²) were hidden beneath the cranial bones. Only 51.4 mm² (SD: 9.9 mm²) of the left hemisphere and 40.6 mm² (SD: 11.0 mm²)of the right hemisphere were visible on average. The majority of the left (MV: 256.2 mm², SD: 21.0 mm²) and right (MV: 276.8 mm², SD: 23.5 mm²) hemisphere was not accessible through the standard approach. The overflow area is not listed in Tab. 7 as it was very similar to the one listed in Tab 6.

Tab. 6: Visible and non-visible areas of the cerebellum through the standard approach in mm²

	Cerebellum not visible	Overflow visible	Cerebellum visible
Cat 1 App1	586.5	15.9	224.6
Cat 2 App1	605.5	17.4	241.6
Cat 3 App1	648.1	18.1	197.2
Cat 4 App1	550.3	6.9	170.1
Cat 5 App1	718.7	9.6	186.6
Cat 6 App1	664.4	25.2	220.7
Cat 7 App1	644.4	11.6	199.4
MV	631.2	14.9	205.7
SD	55.4	6.1	24.6

Tab. 7: Visible and non-visible areas of the compartments of the cerebellum through the standard approach in mm²

	Vermis	HemL	HemR	Vermis	HemL	HemR
	not visible			visible		
Cat 1 App1	94.8	237.2	260.1	115.9	60.8	42.9
Cat 2 App1	73.9	258.1	275.1	125.0	56.6	57.3
Cat 3 App1	117.0	251.3	276.8	107.9	57.9	29.9
Cat 4 App1	74.7	228.6	244.3	84.4	54.3	30.8
Cat 5 App1	108.0	291.8	318.1	90.2	51.7	43.3
Cat 6 App1	108.3	255.5	291.8	145.9	31.4	50.6
Cat 7 App1	103.0	271.3	271.1	120.7	47.2	29.5
MV	97.1	256.2	276.8	112.9	51.4	40.6
SD	16.9	21.0	23.5	21.0	9.9	11.0

4.5 Visible and non-visible areas through the extended approach to the left

The same procedure done for the standard approach was carried out for the extended approach to the left. The measurements are listed in Tab. 8 and 9. A mean value of 355.8 mm² (SD: 40.4 mm²) of the cerebellar surface was visible through this craniotomy window. On average 481.1 mm² (SD: 36.7 mm²) were still covered by the cranial bones. The overflow area consists of part of the *Medulla oblongata* and part of the caudal cerebrum. On average, the extended approach to the left increases the area of visible vermis to 155.1 mm² (SD: 30.2 mm²) and the area of visible left hemisphere to 158.0 mm² (SD: 23.5 mm²). The accessibility of the right hemisphere stays not surprisingly almost the same compared to the standard approach, with a mean value of 40.9 mm² (SD: 11.1 mm²).

Tab. 8: Visible and non-visible areas of the cerebellum through the extended approach to the left in mm²

	Cerebellum not visible	Overflow visible	Cerebellum visible
Cat 1 App2left	423.1	22.6	388.0
Cat 2 App2left	491.1	132.4	356.1
Cat 3 App2left	497.2	135.4	348.1
Cat 4 App2 left	444.3	101.1	276.1
Cat 5 App2left	534.4	68.8	370.9
Cat 6 App2left	483.7	118.8	401.4
Cat 7 App2left	493.8	102.3	350.0
MV	481.1	97.3	355.8
SD	36.7	39.9	40.4

Tab. 9: Visible and non-visible areas of the compartments of the cerebellum through the extended approach to the left in mm²

	Vermis	HemL	HemR	Vermis	HemL	HemR
	not visible			visible		
Cat 1 App2left	54.8	118.2	259.8	155.9	179.8	43.2
Cat 2 App2left	31.9	185.3	274.8	167.0	129.4	57.6
Cat 3 App2left	74.8	141.2	277.6	150.1	168.0	29.2
Cat 4 App2 left	50.6	147.1	243.7	108.5	135.8	31.3
Cat 5 App2left	63.1	150.6	318.6	135.1	192.9	42.8
Cat 6 App2left	47.3	143.4	290.9	206.9	143.5	51.5
Cat 7 App2left	61.5	162.1	269.8	162.2	156.4	30.7
MV	54.9	149.7	276.5	155.1	158.0	40.9
SD	13.6	20.5	23.7	30.2	23.5	11.1

4.6 Visible and non-visible areas through the extended approach to the right

The same procedure as described in 4.4 and 4.5 was executed for the extended approach to the right. On average 370.4 mm² (SD: 44.2 mm²) of the cerebellar surface was visible through the craniotomy window and an average of 466.5 mm² (SD: 52.8 mm²) were not visible. This approach increased the accessibility of the vermis to a mean value of 156.5 mm² (SD: 26.5 mm²). A mean value of 161.8 mm² (SD: 25.5 mm²) of the right approach was visible through the bony defect. The accessibility of the left hemisphere almost stays the same as in the standard approach with a mean value of 50.7 mm² (SD: 10.0 mm²).

Tab. 10: Visible and non-visible areas of the cerebellum through the extended approach to the left in mm²

	Cerebellum not visible	Overflow visible	Cerebellum visible
Cat 1 App2right	376.4	21.1	434.6
Cat 2 App2right	478.7	156.2	368.5
Cat 3 App2right	460.7	95.4	384.6
Cat 4 App2right	426.7	81.6	293.7
Cat 5 App2right	541.2	72.9	364.0
Cat 6 App2right	484.7	140.8	400.4
Cat 7 App2right	497.1	71.4	346.7
MV	466.5	91.3	370.4
SD	52.8	45.5	44.2

Tab. 11: Visible and non-visible areas of the compartments of the cerebellum through the extended approach to the right in mm²

	Vermis	HemL	HemR	Vermis	HemL	HemR
	not visible			visible		
Cat 1 App2right	37.6	238.1	109.2	173.1	59.9	193.8
Cat 2 App2right	37.1	258.5	180.0	161.8	56.2	152.4
Cat 3 App2right	52.1	251.6	153.0	172.9	57.5	153.8
Cat 4 App2right	47.1	228.3	148.5	112.0	54.7	126.6
Cat 5 App2right	69.6	293.1	178.2	128.6	50.4	183.2
Cat 6 App2right	68.1	256.0	158.4	186.1	30.9	184.0
Cat 7 App2right	62.7	273.1	162.1	161.0	45.3	138.5
MV	53.5	257.0	155.6	156.5	50.7	161.8
SD	13.7	21.5	23.7	26.5	10.0	25.5

4.7 Visibility and removed bone in percentage

After the previously described values were measured, the following parameters, listed in Tab. 12 to 14, were calculated. For the standard approach, an average of 26.5 % of the occipital bone was removed. The percentage of bone that was removed for the extended approaches was not calculated, as it also affected the parietal bone that was not measured.

On average 24.6 % of the cerebellum was visible through the craniotomy window of the standard approach. That equals 18.2 % of the complete cerebellar surface. Through the extended approach to the left, a mean value of 42.5 % of the cerebellum was accessible, which equates 31.5 % of the whole surface. Through the extended approach to the right a mean value of 44.3 % of the cerebellum was visible, which equates 32.8 % of the whole surface. That means the access to the cerebellum increased by 73.6 % with the extended approach to the left and by 80.6 % with the extended approach to the right.

Tab. 12: Percentage of occipital bone removed for the standard approach and percentage of the accessed cerebellum through the different approaches

	bone/bone App1	% Cerebellum					
		App1	App2 left	App2 right	whole surface		
					App1	App2 left	App2 right
Cat 1	19.2	27.7	47.8	53.6	19.6	33.8	37.9
Cat 2	37.0	28.5	42.0	43.5	21.0	31.0	32.1
Cat 3	22.1	23.3	41.2	45.5	18.7	33.0	36.4
Cat 4	30.4	23.6	38.3	40.8	17.2	27.9	29.7
Cat 5	25.4	20.6	41.0	40.2	15.9	31.6	31.0
Cat 6	27.1	24.9	45.4	45.2	17.9	32.5	32.4
Cat 7	24.6	23.6	41.5	41.1	17.4	30.5	30.2
Average	26.5	24.6	42.5	44.3	18.2	31.5	32.8
SD	5.8	2.7	3.1	4.6	1.7	1.9	3.1

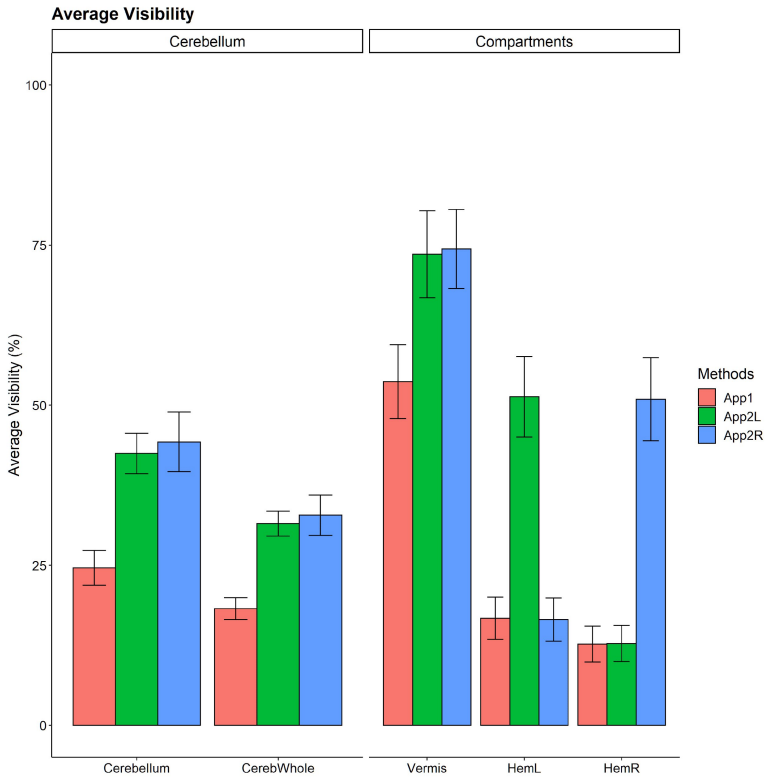

Fig. 18: Average visibility of the Cerebellum and its compartments through the different approaches, error bars correspond to one standard deviation

A mean value of 53.7 % of the vermis was accessible through the standard approach. Through the extended approach to the left an average of 73.6 % of the vermis was visible, which equates an increase of 37.4 % compared to the standard approach. The results for the extended approach to the right were very similar with an average of 74.4 % of the vermis visible, which means an increase of 39.3 % compared to the standard approach. Through the

standard approach an average of 16.7 % of the left hemisphere was accessible. Through the extended approach approximately half of the left hemisphere was visible, meaning an average increase of 218.0 %. Naturally the visibility of the right hemisphere through the extended approach to the left did not increase compared to the standard approach. The small numbers listed in Tab. 14 for the percentage increase of the extended approach the left concerning the right hemisphere, are due to imprecision of the measuring process and can be discarded. Simultaneously to that, the extended approach to the right caused an average increase in visibility of the right hemisphere of 314.2 %, making an average of 50.9 % of the right hemisphere accessible. Obviously, the extended approach to the right does not cause an increase in visibility of the left hemisphere and the calculated values can also be discarded.

Tab. 13: Percentage of vermis, left and right hemisphere visible through the different approaches

	% Vermis			% Hemisphere					
	App1	App2 left	App 2 right	left			right		
				App1	App2 left	App2 right	App1	App2 left	App2 right
Cat 1	55.0	74.0	82.2	20.4	60.3	20.1	14.2	14.3	64.0
Cat 2	62.9	84.0	81.3	18.0	41.1	17.9	17.2	17.3	45.8
Cat 3	48.0	66.7	76.9	18.7	54.3	18.6	9.8	9.5	50.1
Cat 4	53.1	68.2	70.4	19.2	48.0	19.3	11.2	11.4	46.0
Cat 5	45.5	68.2	64.9	15.1	56.2	14.7	12.0	11.9	50.7
Cat 6	57.4	81.4	73.1	10.9	50.0	10.8	14.8	15.0	53.7
Cat 7	54.0	72.5	72.0	14.8	49.1	14.2	9.8	10.2	46.1
Average	53.7	73.6	74.4	16.7	51.3	16.5	12.7	12.8	50.9
SD	5.8	6.8	6.2	3.3	6.3	3.4	2.8	2.8	6.5

Tab. 14: Percentage increase in access in the extended approach to the right and left compared to the standard approach

	App2 left	App2 right	App 2 left			App 2 right		
	Cerebellum		Vermis	HemL	HemR	Vermis	HemL	HemiR
Cat 1	72.8	93.5	34.5	195.7	0.7	49.4	-1.5	351.6
Cat 2	47.4	52.5	33.6	128.7	0.6	29.4	-0.7	166.1
Cat 3	76.6	95.1	39.0	190.2	-2.6	60.1	-0.6	414.0
Cat 4	62.3	72.7	28.5	149.9	1.8	32.6	0.6	311.4
Cat 5	98.8	95.1	49.8	273.0	-1.0	42.6	-2.6	323.6
Cat 6	81.9	81.4	41.8	356.9	1.7	27.5	-1.5	263.5
Cat 7	75.6	73.9	34.4	231.3	4.2	33.3	-4.0	369.4
Average	73.6	80.6	37.4	218.0	0.8	39.3	-1.5	314.2
SD	16.0	15.7	6.9	77.9	2.1	12.0	1.5	80.6

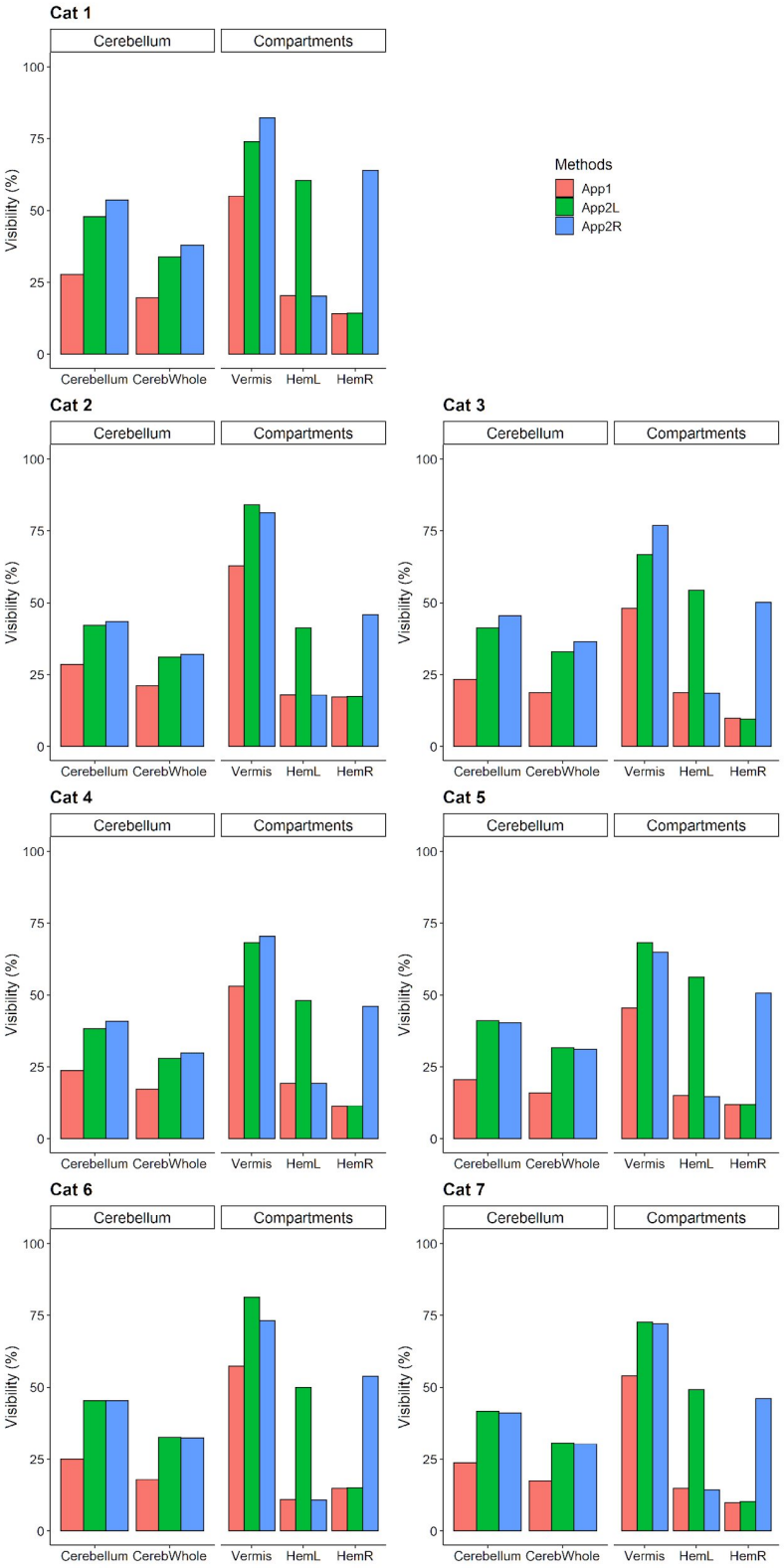

Fig. 19: Visibility of the Cerebellum and its compartments through the different approaches from all seven cats,compared to the visibility with all cranial bones removed, in percentage, the red bar represents the standard approach, the green bar represents the extended approach to the left side and the blue bar the extended approach to the right side; Cerebellum stands for the visible cerebellar surface with the Cerebrum in situ, Cereb/Whole stands for the whole cerebellar surface, the compartments are subdivided into vermis, left hemisphere (HemL) and right hemisphere (HemR)

5 Discussion

Up till now, only little information on suboccipital craniotomy approaches in cats is available. In order to describe bony landmarks to standardize the maximal expansion of the approach and gather information about the accessibility of the cerebellum and its parts, virtual suboccipital craniotomies were carried out in seven cats in this study. Furthermore, to register the increase in accessibility of the cerebellum with a rostrolateral extended approach, a combined rostrotentorial and suboccipital approach was executed in each of the cats on both sides. Only the data of cats, that received MRI and CT scans for other reasons than brain pathologies, were used, so that similarity of the anatomical structures is guaranteed.

Due to the variety of possible expansions of the suboccipital approach, corresponding to the indication, it is difficult to find recommendations on the exact placement of drill holes, in current literature. In order to maximize the craniotomy window without insulting the transverse sinus or the confluens sinuum, the drill holes in this study were placed just ventrally to the nuchal crest and the *Protuberantia occipitalis.* The bony defect is then continued ventrally to the *For. magnum*, removing an average of 26.5 % of the occipital bone. In order to carry out a combined rostroentorial and suboccipital approach, two additional drill holes are described using palpable anatomical landmarks. The first one 5 mm lateral to the rostral end of the *Crista saggitalis* and the second one 1 cm dorsal to the caudal edge of *Processus mastoideus.* As a moderate amount of the caudal cerebrum is also visible through a craniotomy window with these drill holes, they could be placed a little more caudally in real life.

Even though the standard approach in this study was maximized, only an average of 24.6 % of the cerebellar surface, which corresponds to 18.2 % of the whole surface of the cerebellum, was visible. Due to the caudal midline location of the approach, naturally mostly the vermis is visible. To be more specific, on average 53.7 % of the vermis is accessible through the standard approach. Due to the slight asymmetry of the cerebellar compartments, the left hemisphere (MV: 16.7 %) is marginally more accessible through the standard approach than the right hemisphere (MV: 12.7 %).

One of the most common indications for intracranial surgery in cats is the removal of tumors, such as meningioma (Troxel et al 2003). In order to reach masses in the rostrolateral parts of the cerebellum and the cerebellopontine angle or in order to successfully remove larger masses, an extension of the suboccipital approach is necessary. This study showed that a rostrolaterally extended approach increases the accessibility of the cerebellum by 73.6 % to the left side and 80.6 % to the right side compared to the standard suboccipital approach.

The access to the hemisphere of the ipsilateral side is significantly better, with an increase of 218 % on the left side and 314.3 % on the right side. Given the significant increase in visibility of the cerebellum and its parts, a combined rostrotentorial and suboccipital approach should be considered in patients with harder to reach tumors, even though transverse sinus occlusion, which is tied to the laterorostral extension, comes with a higher risk of surgical complications. Furthermore studies on the transverse sinus occlusion in dogs, showed that the ICP is not negatively affected after the permanent ligation of the transverse sinus, if a craniectomy is executed. (Bagley et al. 1997, Pluhar et al. 1996)

Due to the large bony defect left after the extended approach, a bony reconstruction is likely necessary. This can be achieved by repositioning of the previously preserved bone flap. If the bone flap cannot be used, other methods to reconstruct the calvarium are described. For example the use of PMMA or a gamma-irradiated calvarial allograft have been described in dogs and cats. Furthermore the placement of contourable titanium mesh has lead to successful closure of the canine and feline calvarium. (Langley-Hobbs et al. 2014, Shores and Brisson 2017, O´Brien et al. 2010, Langer et al. 2018)

5.1 Limitations

Even though the subject group is rather small, the collected data is useful to give an estimate on how much of the cerebellum and its parts is accessible through the different approaches.

Due to the small size of cat skulls, the resolution of the MR images is lower compared to dogs and humans. This causes slight inaccuracy in the 3D reconstruction of the brain. Furthermore due to the surface visualization as triangles in the Amira® software and the manually marked areas, extreme preciseness is not possible. Therefore all measurements should be viewed as estimates. Moreover the irregular surface of the occipital bone caused the measured craniotomy window to be slightly bigger than the actual bony defect.

5.2 Conclusion

In conclusion only a small part of the cerebellum and its compartments is visible through the standard suboccipital approach, without insulting the transverse sinus The rostrolateral extension of the approach can significantly increase accessibility of the cerebellum. The access to the ipsilateral hemisphere is even increased by more than 200 % compared to the standard approach. Further studies are necessary to determine the practicality of transverse sinus occlusion in cats. As the availability of diagnostic imaging and surgical treatment options for intracranial tumors in veterinary medicine is continuously increasing, further

studies concerning craniotomy approaches in real life cats will be necessary to optimize surgical techniques.

6 Summary

For this diploma thesis, the CT and MRI scans of seven cats without brain pathologies were used retrospectively, to virtually carry out suboccipital craniotomy approaches. Bony landmarks, that enable a maximum expansion of the standard suboccipital approach without insulting vital structures, were described. Also the difference in accessibility of the cerebellum between a standard suboccipital approach and a rostrolaterally extended approach on the left and on the right side, respectively, was captured.

Using the Amira® software to process the imaging data, 3D models of the feline skull and brain were created. Craniotomy windows were virtually cut and the accessible underlying area of the cerebellum and its parts was measured. The measurements were then put into relation with the previously measured entire surface of the cerebellum and its parts.

The results show, that an average of 26.5 % of the occipital bone is removed for the maximum extension of the standard approach. Furthermore they show, that only 24.6 % of the cerebellar surface is visible through the standard approach. A rostrolateral extension to the left side increases the accessibility of the cerebellum by 73.6 % and 80.6 % to the right side compared to the standard suboccipital approach. The access to the ipsilateral hemisphere is even increased by more than 200 %. Given the significant increase in visibility, a transverse sinus occlusion, which is tied to the rostrolateral extension, should be considered in harder to reach tumors.

7 Zusammenfassung

Für diese Diplomarbeit wurden die CT- und MRT-Daten von sieben Katzen ohne Hirnpathologien retrospektiv verwendet, um virtuell subokzipitale Kraniotomiezugänge durchzuführen. Es wurden knöcherne Orientierungspunkte beschrieben, die eine maximale Ausdehnung des subokzipitalen Standardzugangs ermöglichen, ohne vitale Strukturen zu verletzen. Auch der Unterschied in der Zugänglichkeit des Kleinhirns zwischen einem suboccipitalen Standardzugang und einem rostrolateral erweiterten Zugang auf der linken bzw. rechten Seite wurde erfasst.

Mit Hilfe der Amira®-Software zur Verarbeitung der Bildgebungsdaten wurden 3D-Modelle des felinen Schädels und Gehirns erstellt. Die Kraniotomie-Fenster wurden virtuell ausgeschnitten und die zugängliche Oberfläche des Kleinhirns und seiner Teile wurde vermessen. Die Messungen wurden dann mit der zuvor gemessenen Gesamtoberfläche des Kleinhirns und seiner Teile in Beziehung gesetzt.

Die Ergebnisse zeigen, dass bei der maximalen Ausdehnung des Standardzugangs durchschnittlich 26,5 % des Hinterhauptbeins entfernt werden. Außerdem zeigen sie, dass nur 24,6 % der Kleinhirnoberfläche durch den Standardzugang sichtbar ist. Eine rostrolaterale Erweiterung auf der linken Seite erhöht die Zugänglichkeit des Kleinhirns um 73,6 % und um 80,6 % auf der rechten Seite im Vergleich zum subokzipitalen Standardzugang. Der Zugang zur ipsilateralen Hemisphäre wird sogar um mehr als 200 % verbessert. Angesichts der deutlich verbesserten Sichtbarkeit sollte bei schwer zugänglichen interkranialen Tumoren ein Verschluss des transversalen Sinus, der bei einer rostrolateralen Erweiterung unumgänglich ist, in Betracht gezogen werden.

8 References

Bagley RS Harrington ML, Pluhar GE, Gavin PR, Moore MP. 1997. Acute, Unilateral Transverse Sinus Occlusion During Craniectomy in Seven Dogs With Space-Occupying Intracranial Disease. Veterinary Surgery, 26:195-201.

Cameron S, Rishniw M, Miller AD, Sturges B, Dewey CW. 2015. Characteristics and Survival of 121 Cats Undergoing Excision of Intracranial Meningiomas (1994–2011). Veterinary Surgery 44: 772–776.

Constantinescu GM. 2018. Illustrated Veterinary Anatomical Nomenclature. Forth Edition. Stuttgart: Enke Verlag.

Di Ieva A, Lee JM, Cusimano MD. 2016. Handbook of Skull Base Surgery. New York: Thieme Medical Publisher Inc., 391-398.

Filgueiras R. 2016 https://www.vin.com/apputil/content/defaultadv1.aspx?pId=19840&catId=105889&id=8249789&ind=500&objTypeID=17 (Zugriff 03.08.2022).

Fossum TW. 2019. Small animal surgery. Fifth edition. Philadelphia: Elsevier, Inc., 1338-1364.

Greenberg MS. 2016. Handbook of Neurosurgery. Eight Edition. New York: Thieme Medical Publisher Inc., 681, 1445-1453.

Hudson LC, Hamilton WP. 2010. Atlas of Feline Anatomy For Veterinarians. Teton NewMedia, 28, 194-199.

Kent M, Glass EN, Schachar J. 2020. A lateral approach to the feline cerebellar fossa: case report and identification of an external landmark for the tentorium ossium. Journal of Feline Medicine and Surgery, 22(4):358-365

König HE, Liebich HG. 2005. Anatomie der Haussäugetiere. Stuttgart: Schattauer GmbH, 47-82.

Langer P, Black C, Egan P, Fitzpatrick N. 2018. Treatment of calvarial defects by resorbable and non-resorbable sonic activated polymer pins and mouldable titanium mesh in two dogs: a case report. BMC Veterinary Research, 14(1): 199

Langley-Hobbs SJ, Demetriou JL, Ladlow JF. 2014. Feline Soft Tissue and General Surgery. London: Saunders Elsevier, 707-727.

Maiuri F, Donzelli R, Pagano S, Mariniello G. 2019. The Management of the Venous Sinuses During Surgery for Posterior Fossa meningiomas. World Neurosurgery, 125: 357-363.

Nickel R, Schummer A, Seiferle E. 2004. Lehrbuch der Anatomie der Haustiere. 8. Aufl. Stuttgart: Parey Verlag.

O´Brien CS, Bagley RS, Hicks DG, Chen AV, Wininger FA, Brumitt JW. 2010. Gamma-irradiated Calvarium Allograft Cranioplasty in a cat following brain tumor removal. Journal of the Americam Animal Hospital Association., 46(4): 268-273

Oliver JE. 1968. Surgical approaches to the canine brain. American Journal of Veterinary Research 29:353-378.

Pluhar GE, Bagley RS, Keegan RD, Bazler TV, Moore MP. 1996. The Effect of Acute, Unilateral Transverse Venous Sinus Occlusion on Intracranial Pressure in Normal Dogs. Veterinary Surgery, 25:480-486.

Salomon FV, Geyer H, Gille U. 2015. Anatomie für die Tiermedizin. 3. Aufl. Stuttgart: Enke Verlag.

Sekhar LN, Fessler RG. 2016. Atlas of Neurosurgical Techniques. Second Edition. New York: Thieme Medical Publisher Inc., 247-252.

Shores A, Brisson BA. 2017. Current Techniques in Canine and Feline Neurosurgery. First Edition. Hoboken: John Wiley & Sons, 115-120.

Troxel MT, Vite CH, Van Winkle TJ, Newton AL, Tiches D, Dayrell-Hart B, Kapatkin AS, Shofer FS, Steinberg SA. 2003. Feline Intracranial Neoplasia: Retrospective Review of 160 Cases (1985–2001). Journal of Veterinary Internal Medicine, 17(6):850-859.

Zilli J, Kressin M, Schaenzer A, Kampschulte M, Schmidt MJ. 2021. Partialcortico-hippocampectomy in cats, as therapy for refractory temporal epilepsy: A descriptive cadaveric study. PLoS ONE, 16(1): e0244892

9 Figures and Tables

Acknowledgements

First and foremost, I would like to thank my thesis advisor, Dr. med. vet. Gabriele Gradner, Dipl. ECVS, for her valuable input and constructive feedback.

Furthermore, I would like to thank Dr. Stephan Handschuh, part of the VetCore Facility for Research at the University of Veterinary Medicine Vienna, for his dedicated guidance through the Amira® software. His advice and quick problem solving helped me many times.

Moreover I want to acknowledge Emmanouil Lyrakis, Ph.D., from the Platform for Bioinformatics and Biostatistics. I am very grateful for his assistance with the statistical analysis and for putting my results into adequate charts.

Last but not least I want to express my gratitude to my family and my partner for their patience and never ending support through my studies and the process of writing this thesis. Special thanks to Thomas and Magdalena Szelestey for proofreading. Your feedback was very much appreciated.